HHS Public Access

Author manuscript

Cell Rep. Author manuscript; available in PMC 2016 July 21.

Published in final edited form as:

Cell Rep. 2016 July 19; 16(3): 597–604. doi:10.1016/j.celrep.2016.06.037.

Somatostatin interneurons control a key component of mismatch negativity in the mouse visual cortex

Jordan P. Hamm[1,*] and **Rafael Yuste**[1]

[1]Neurotechnology Center, Department of Biological Sciences, Columbia University, New York, NY, 10027.

Summary

Patients with schizophrenia have deficient sensory processing, undermining how they perceive and relate to a changing environment. This impairment can be captured by the reduced "mismatch negativity" index (MMN), an electroencephalographic biomarker of psychosis. The biological factors contributing to MMN are unclear, though mouse research, where genetic and optical methods could be applied, has given some insight. Using fast two-photon calcium imaging and multielectrode recordings in awake mice, we find that visual cortical circuits display i) adapted (decreased) responses to repeated stimuli and ii) amplified responses to a deviant stimulus, the key component of human MMN. Moreover, pharmacogenetic silencing of somatostatin-containing interneurons specifically eliminated this amplification along with its associated theta/alpha band response, leaving stimulus specific adaption and related gamma-band modulations intact. Our results validate a mouse model of MMN and suggest that abnormalities in somatostatin-containing interneurons cause sensory deficits underlying MMN and schizophrenia.

Graphical Abstract

[*]**Contact Information:** jph2164@columbia.edu.

Author Contributions. Conceptualization, J.P.H. and R.Y.; Methodology, J.P.H.; Investigation, J.P.H.; Writing –Original Draft, J.P.H.; Writing –Review & Editing, J.P.H and R.Y.

EToC blurb:

Hamm and Yuste develop a mouse model of "mismatch negativity", a classic EEG biomarker of schizophrenia. They pinpoint two components of this marker within visual cortex (adaptation and deviance detection), revealing that pharmacogenetic suppression of somatostatin inhibitory neurons specifically eliminates deviance detection, the higher order component critically deficient in patients.

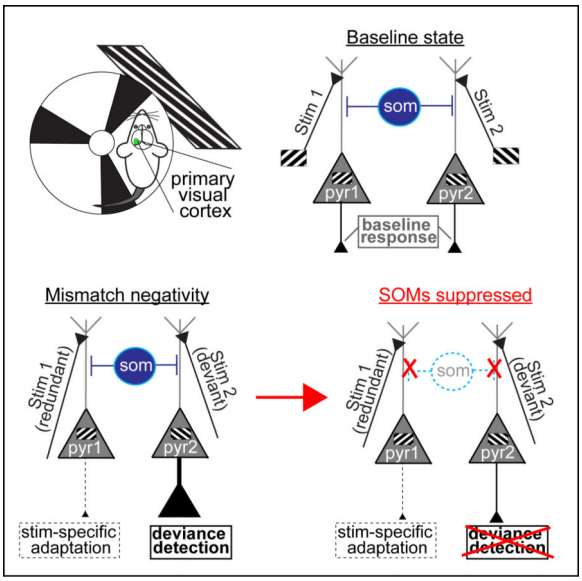

Schizophrenia involves fundamental aberrations in perception and cognition. Deficient neural processing of environmentally salient events may underlie these core symptoms (Javitt and Freedman, 2015). Such deficiencies have been traditionally quantified in schizophrenia patients using electroencephalography (EEG) while employing “oddball” sensory stimulation paradigms. In such experiments, evoked cortical responses to a repetative or “standard” auditory stimulus are compared to a deviant or “target” stimulus. The resulting difference in EEG potentials between the redundant and the deviant stimulus is quantified and termed “mismatch negativity” (MMN). While psychiatrically healthy individuals react to the new, deviant stimulus with an amplified cortical response (or MMN, peaking between 150-250ms post-stim onset), schizophrenic patients show a strongly reduced MMN, as if they did not register the “target” stimulus as “deviant”. A reduced MNN response is a widely replicated biomarker of schizophrenia, showing invariance across sensory modalities and even predicting illness onset in premorbid individuals (Garrido et al., 2009; Light and Näätänen, 2013).

More specifically, the MMN difference potential consists of at least two more basic underlying components: (i) a simple adaptation (reduction) of neural responses to a redundant or repeated stimulus (“stimulus specific adaptation” or SSA), and (ii) an amplified “deviance detection” response, indicating that the rare stimulus violates the expected contextual regularity (Harms et al., 2015). Animal studies show that SSA is present both cortically and subcortically and may reflect synaptic depression in feedforward excitatory inputs (Farley et al., 2010; Garrido et al., 2009). But the neural mechanisms underlying deviance detection, and thus the salience processing deficits thought to underlie the MMN biomarker of schizophrenia, remain unknown.

Understanding whether and how deviance processing is generated in sensory cortex could help link quantifiable biomarkers to the fundamental disease pathophysiology and symptoms. While non-SSA components of MMN are dependent on NMDA-receptor neurotransmission (Farley et al., 2010; Javitt and Freedman, 2015), little consistency exists

regarding the contribution of GABAergic inhibition (Garrido et al., 2009). Examining the causal roles of specific inhibitory interneuron subtypes, rather than GABAergic cells in general, may help advance our understanding of MMN. In particular, somatostatin-containing interneurons (SOMs) display abnormalities in post-mortem brain samples of schizophrenia patients (Hashimoto et al., 2008). SOMs are a strong candidate for MMN processing given their: i) late input/output facilitation (or amplification) in the MMN time-range (Karnani et al., 2014), ii) a capacity for both inhibition and dis-inhibition of neighboring pyramidal neurons (Cottam et al., 2013), and iii) preferential inhibition of the local neuronal network to redundant stimuli compared to deviants (Natan et al., 2015). These characteristics lie in contrast to other more commonly studied interneuron types, such as parvalbumin containing cells (Cottam et al., 2013; Karnani et al., 2014; Natan et al., 2015; Zhu et al., 2015).

The use of genetically engineered “cre-driver” mice would enable the investigation of neocortical SOM involvement in MNN directly (Cottam et al., 2013). Studies employing basic oddball paradigms have shown that MMN-like waveforms (deviant minus redundant) are present in mouse EEG recordings (Featherstone et al., 2015), but an analytical and mechanistic differentiation of higher order deviance processing from basic sensory adaptation (SSA) is absent, leaving the translational relevance to human MMN unclear (Harms et al., 2015). Some recent studies focusing on SSA have made use of mouse strains allowing interneuron access with optogenetics or florescent microscopy (PV-cre, SOM-cre). Natan et al (2015) quantified SSA from extracellular spiking in auditory cortex (A1) of anesthetized mice and showed that both SOMs and PVs play a role in SSA, but deviance detection was not examined in this study and a link to MMN was never claimed. Using patch recordings, again in anesthetized mouse A1, Chen et al (2015a) focused mainly on SSA but found some evidence of subthreshold deviance detection in pyramidal neurons in tertiary experiments. Spiking outputs nevertheless failed to show deviance detection in this setup, leaving the question of whether rodent neocortical circuits generate or even passively relay deviance related, human-like MMN signals uncertain at best.

Results

Here we demonstrate that key MMN components, SSA and deviance detection, are quantitatively and mechanistically differentiable in mouse cortical circuits. Unlike past work, we study awake animals, a potentially important experimental difference because the activity of SOMs in particular is strongly suppressed under anesthesia relative to awake conditions (Gentet et al., 2012). Further, we focus on primary visual cortex since neurons of specific orientation selectivity are intermixed in mouse V1 (Niell and Stryker, 2008), allowing for localized recordings of both adapted and facilitated populations simultaneously in a simple oddball paradigm. Using targeted pharmacogenetics (Designer Receptors Exclusively Activated by Designer Drugs; D.R.E.A.D.D.S), we further show that a deficit in SOMs, a known component of schizophrenia pathophysiology, could be causally related to the MMN biomarker and affect related oscillatory dynamics in the theta/alpha band.

Stimulus adaption and deviance detection can be detected in mouse cortical circuits

We performed i) multielectrode recordings with current source density (CSD) analysis (see below) to measure localized synaptic activities (Buzsáki et al., 2012) and ii) fast two-photon resonance imaging (30-Hz) of florescent calcium indicators (GCaMP6s/f) to infer spiking activity in populations of individual neurons simultaneously and stably in awake, head-fixed mice (C57BL/6 background; n=31; Fig 1a; S1). We included three 10-15 minute stimulus presentations (Fig 1b): i) oddball with 12.5 % "deviant" full-field squarewave gratings of 45-deg intermixed with 87.5% "redundants" of 135-deg, ii) oddball with stimulus reversal (135-deg deviants), and iii) a "many standards" control sequence with 8 orientations (0-180-deg) each occurring 12.5% of the time. We then quantified cortical responses to the same stimulus across contexts wherein it is i) redundant, ii) rare and contextually deviant, and iii) rare but not deviant ("many standards" control), equating the number of trials across conditions. Comparing (i) to (iii) yields an estimate of SSA, while (ii) to (iii) estimates deviance detection (Harms et al., 2015).

Local field potentials (LFP) were recorded from 16 linearly arranged sites on a silicon probe (Fig. 1c; spaced 50μm for 750μm). Past studies of MMN in humans have typically compared EEG responses magnitudes between deviant and redundant stimuli directly, or generated a difference score to be compared between diagnostic groups (Javitt and Freedman, 2015). Here, average stimulus-evoked LFP traces (Fig. 1d, S1a) showed a protracted deviant greater than redundant effect in mid to late time latencies (40-240 ms, $t(13)=-2.19, p<.05$) which, similar to human MMN, peaked between around 120-240 ms (LFP-MMN; fig 1d right; plots and analyses are computed averaging over stimulus orientations unless otherwise stated). The LFP, like EEG, is spatially imprecise, convolving activity from 0.5-1cm^2 involving neighboring layers, columns, and, thus, in mice, other brain regions (Buzsáki et al., 2012). To examine underlying components of this effect at the circuit level, LFPs were transformed to CSD by computing the discrete second spatial derivative (Fig. 1d). Consistent with previous CSD recordings in mouse V1, we identified a large current sink at approximately 400 um from the surface, flanked by later current sources in superficial and deeper regions, which may correspond to granular, supragranular, and infragranular cortical regions given their concordance with previously verified histological work and highpass filtered "multiunit" activity (Fig. S1a; see methods). Regardless of cortical depth, we found clear evidence of SSA, mainly within an earlier time range (40-80ms), and, in a later time range (120-240ms), clear evidence of deviance detection (Fig. 1e). After rectifying averages and combining across layers, we confirmed statistically smaller responses to redundant ($t(13)=3.24$, $p<.01$) and greater responses to deviant ($t(13)=-2.94$, $p<.01$) than control (putative SSA and deviance detection; Fig. 1f).

We then used two-photon calcium imaging (2P-Ca^{2+}) to measure spiking activity of populations of neurons in layer 2/3 of V1 (820 neurons total across 18 mice; Fig. 1g). We quantified frame to frame changes in florescence (delta-f) converted to z-scores based on baseline signal fluctuation (see methods). Approximately 19% of all recorded neurons (n=160) displayed an increase in activity of greater than 1.67 stdev above pre-stim baseline

(1-tailed probability p<.05; Fig. 1h; S2) to one of the two key stimulus orientations in either the control or deviant condition. Among these cells we observed a clear reduction in activity, relative to control, when its preferred stimulus was redundant ($t(159)=5.40$, p<.01; Fig. 1i,j; S2); and a marked increase in responses when its preferred stimulus was contextually deviant ($t(159)=-2.73$,p<.01; Fig. 1i,j; see S1c-d for further validation). These effects were consistent with electrophysiological multiunit activity (unsorted population spiking) acquired with the multielectrode (Fig. S1b). Thus, using this visual oddball paradigm, an MMN-like LFP response was present, and key underlying components, SSA and deviance detection, could be measured and differentiated in mouse V1.

Silencing SOMs disrupts deviance detection but not SSA

Given our ability to measure and differentiate MMN components in this mouse model, we next explored potential local circuit elements contributing to these phenomena. Given the specialized functional properties of SOMs compared to other interneuron types (see above, we tested whether the MMN-like response we observed in mouse V1 were dependent on SOM activity by using a pharmacogenetic approach (DREADDS), virally targeting SOMs in a SOM-cre mouse line to express inhibitory channel hM4D (Fig S3). hM4D activation by Clozapine N-Oxide (CNO; a naturally inert ligand) functionally silences host cells primarily through the suppression of synaptic current amplitude and release (see supplement). We quantified CSDs and 2P-Ca^{2+} dynamics before and 30 minutes after subcutaneous injection of CNO (12 mg/kg CNO) in SOM-hM4D mice (n=11) or controls (n=9). Immunohistochemistry confirmed the specificity of hM4D-mCherry construct to SOM interneurons across all cortical depths (Fig. S3), and 2P-Ca^{2+} dynamics recording in a dark room during non-locomotive rest also confirmed a generalized disinhibition of the local network after SOM-suppression (Fig. S4a-c), but did not significantly alter the frequency of locomotion ($F(1,10)^{\text{SOM-hM4D}}=.82$, p=.38).

Traditional MMN analysis of average LFP values (deviant minus redundant) in the 120-240ms time-range suggested that SOM suppression disrupted MMN-like responses (Fig 2, showing a GROUP×TREATMENT interaction ($F(1,7)=6.08$, p<.05; $F(1,4)^{\text{CNO-control}}=0.04$, p=.85, $F(1,4)^{\text{SOM-hM4D}}=8.53$, p<.05; Fig 2a,b,f,g). Early latency SSA (40-80ms) was not affected by SOM suppression (control-minus-redundant; GROUP×TREATMENT $F(1,7)=0.13$, p=.72;$F(1,3)^{\text{CNO-control}}=1.54$, p=.30; $F(1,4)^{\text{SOM-hM4D}}=0.00$, p=.97; Fig 2c,d,h,i). On the other hand, deviance detection, particularly in the time range of the MMN (120-240ms), was strongly diminished after SOM suppression (deviant-minus-control; GROUP×TREATMENT $F(1,7)=5.75$, p<.05; $F(1,4)^{\text{SOM-hM4D}}=7.56$, p=.05; $F(1,3)^{\text{CNO-control}}=0.03$, p=.87; Fig 2c,e,h,j). This pattern of effects was mirrored in 2P-Ca^{2+} (top 40 neurons plotted in Fig. 3a,b). The proportion of active neurons expressing deviance detection, but not SSA, was decreased after CNO treatment only in SOM-hM4D (Log-rank$^{\text{deviance-detection}}$-p=.01; $\chi^2=6.16$; Fig 3c,d). Focusing analyses on the top 10% of active neurons pre-treatment to each stimulus, SSA was not affected by SOM-suppression (consistently weaker average responses relative to control magnitude across conditions; $F(1,42)=0.44$, p=.51) but deviance detection showed a GROUP×TREATMENT interaction ($F(1,42)=7.81$, p<.01) which was driven by a treatment effect in the SOM-hM4D group only ($F(1,13)^{\text{SOM-hM4D}}=12.0$, p<.01; $F(1,29)^{\text{CNO-control}}=0.36$, p=.55; Fig 3e, normalized by pre-treatment response). These

results held true for non-normalized values (Fig S4g,h). SOM suppression, importantly, did not alter evoked calcium transients to control stimuli in responsive neurons (first 500ms, $F(1,64)^{\text{SOM-hM4D}}$ =1.66, p=.20; Fig S4d-h), but did produce a trend-level increase in responses to non-preferred stimulus orientations ($F(1,89)^{\text{SOM-hM4D}}$ =3.24, $p=.07$; repeated measures ANOVA on magnitudes 90 deg from peak response; Fig S4d), Previous work has reported either small increases (Zhu et al., 2015) or no change in neuronal responses to visual stimuli after SOM-suppression (Chen et al., 2015b), consistent with their concurrent roles in subtractive inhibition and pyramidal cell disinhibition in V1 (Cottam et al., 2013).

These data thus demonstrated that blocking SOM function selectively reduces deviance detection in cortical circuits without substantively affecting average cell or circuit-level responses at baseline or to redundant stimuli.

Deviance detection responses are generated by SOMs in the theta/alpha band

LFP or EEG recordings of neocortical sensory-evoked responses capture not only large transient events but also dynamic changes in oscillatory power, which reflect population-level synchrony at multiple timescales and frequencies. While other GABAergic interneurons, particularly fast-spiking parvalbumin-containing cells, generate population-level synchrony in the gamma-band, converging evidence suggest that SOMs may play a similar role in lower bands, including theta/alpha (4-14 Hz) or beta (15-30Hz; (Womelsdorf et al., 2014)). Indeed, in awake mice, SOM interneurons show spontaneous and evoked firing rates in the 4-20Hz range (Cottam et al., 2013; Gentet et al., 2012). We reasoned if SOMs were indeed supporting human-like MMN and deviance detection it should be most apparent in LFP recordings of stimulus elicited oscillations in sub-gamma bands.

We adopted a spectral analytical approach previously optimized on clinical EEG data from schizophrenia patients in order to maximize translational potential (see supplement). We converted single trial LFP traces from putative granular layers (the location of the strongest LFP response; Fig. S1) to time/frequency power spectra using a modified-morlet wavelet approach (4-120Hz; 2Hz steps, 1-14 cycles, 5ms steps from −50 to 450ms poststim; averaged across trials and within conditions in fig. 4a). For SSA, redundants evoke significantly lower (30-450ms) gamma power (34-60Hz) than responses to controls ($F(1,8)=22.5$, $p<.01$; Fig. 4b-d), but there was no effect of SOM suppression (i.e. no interaction effects; Fig. 4b-d). For deviance detection responses, there was a STIMxTREATMENT interaction only for theta/alpha power (deviants-vs-control, pre-vs-postCNO; $F(1,8)=8.56$, $p<.05$). Significantly enhanced low-frequency power for deviants was present before ($t(4)=-2.70$, $p<.05$) but not after ($t(4)=1.27$, n.s.; Fig 4 e-f). Together these findings further establish i) the quantitative and mechanistic differentiability of SSA and deviance detection, and ii) a stronger link of SOMs to schizophrenia pathophysiology observed in human EEG studies (Clementz et al., 2016).

Discussion

Our results demonstrate that deviance processing, a critical component of the MMN biomarker of psychosis, is present in V1 circuits in awake mice and depends on the activity of somatostatin-containing interneurons. These findings suggest a causal link in schizophrenia between SOM abnormalities seen in postmortem studies, low frequency population oscillatory dynamics, and deficits in salience processing in patients. Future work will be needed to identify new inroads for therapeutic rescue of sensory deficits, and may uncover further fine-scale mechanistic details for how SOMs exert this control. While it is unlikely that PV containing cells contribute similarly to MMN (Natan et al., 2015), other neocortical cell-types (e.g. vasoactive interstitial peptide neurons (Karnani et al., 2014)) and modulatory neurotransmitters (e.g. acetylcholine (Chen et al., 2015b)) may also play key mediating or moderating roles in the SOM-deviance detection relationship.

It should be noted while a majority of studies in patients have quantified MMN in the auditory domain, visual MMN and visual processing is not spared in schizophrenia (Garrido et al., 2009; Javitt and Freedman, 2015). Caution should nevertheless be taken when equating sensory modalities in a one-to-one manner between species; our results present an animal model for investigating psychotic biomarkers and sensory-cortical microcircuitry in general. As an additional point of consideration, some slight but non-significant long term, pre-vs-post-CNO decreases in evoked activity responses were seen across all measures (LFP, CSD, and calcium transients) which may reflect longer term adaptation effects (Fig 2, S4f-i) or even CNO-administration (though this is unlikely (Roth, 2016)). These did not differ as a function of condition (i.e. SOM suppression), and clearly did not alter the relative magnitudes of the constructs of interest (MMN, deviance detection, and SSA) but may nevertheless be an important topic for future study.

By linking the somatostatin interneurons to deviance detection, and thus the generation of human-like MMN, our data provide a mechanistic entry point into the pathophysiology of schizophrenia and associated sensory/ cognitive dysfunction. The fact that SOMs and MMN affect most directly low frequency bands in the evoked response is in line with the majority of EEG research suggesting that theta/alpha disruptions in schizophrenia are more consistent, heritable, and carry larger effect sizes when compared to beta or gamma (Moran and Hong, 2011). Also, the fact that gamma-band power was neither altered by SOM-suppression nor tracked with deviance detection is also in line with the notion that PV-interneurons do not play a similar role in these phenomena (Womelsdorf et al., 2014). Linking specific pathophysiology like SOM abnormalities to empirical biomarkers such as the MMN may help future attempts at reclassifying psychotic disorders (Clementz et al., 2016) and potentially enable therapeutic approaches at the local microcircuit level.

Experimental Procedures

A detailed description of experimental procedures and rationale are provided in *Supplemental Experimental Procedures*.

Animals, Surgery, and Training

All experimental procedures were approved by and carried out in accordance with Columbia University institutional animal care guidelines. Experiments were performed on adult parvalbumin-cre (n=10) or somatostatin-cre transgenic mice (n=21; Jackson Laboratory, C57BL/6 background, 22-32g; n-31 total), at the age of postnatal day (P) P60-P90. Virus injection, titanium head plate fixation (see supplement), and skull-thinning/craniotomy were carried out in that order over the course of 4 weeks. A glass capillary pulled to a sharp micropipette was advanced with the stereotaxic instrument (coordinates from lambda: X= −2500, Y=200 μm), and 75ul solution of 1:1 diluted AAV1/Syn:GCaMP6s/f (obtained from the University of Pennsylvania Vector Core; n=20) or a 3:7 mixture of AAV1/Syn:GCaMP6s/f and AAV5hsynDIOhM4D(Gi)mCherry (UNC vector core; n=11 SOM-cre mice) was injected into putative layer 2/3 over a 5 min period at a depth of 200-300 μm from the pial surface using a UMP3 microsyringe pump (World Precision Instruments).

On the day of the experiment, the mouse was anesthetized again with isoflurane. For local field potential recordings, a small region (approximately 0.5 mm in diameter) was removed left V1 centered just anterior to the injection site. For calcium imaging experiments, a small circle (approximately 1 mm in diameter) was thinned with a dental over the left V1 centered just anterior to the injection site. The skull was thinned until the bone, moistened with saline, was transparent enough so that the underlying vasculature was visible to the naked eye (usually 10 minutes of drilling). The mouse was then allowed to wake up and was transferred to the wheel for recordings.

Multielectrode recordings

Extracellular electrophysiological data are reported on 14 mice (8 female, 22-28g, 5 PV-cre, 8 SOM-cre). Sixteen-channel linear silicon probes (spaced at 50 Um intervals; model a1x16-3mm50-177, Neuronexus Technologies, Ann Arbor MI) were inserted perpendicular to and with the top electrode aligned just at the pial surface (visually confirmed with an adjustable miniature digital microscope (adafruit)). Recordings were referenced to the skull above prefrontal cortex and grounded to the headplate. Continuous data were acquired with a Plexon MiniDigi amplifier and software (Plexon Inc, Dallas, TX). Local field potential (LFP) signals were filtered from 0.5 to 300Hz and sampled at 1kHz. Single electrodes with the peak negative deflection 50-200ms post-stim near putative granular cortex were reserved for LFP analysis, or the whole array was analysed as current source density (see below). Locomotion was recorded as stripes in the running wheel crossed between an infared LED/photodarlington pair (see supplement).

Two-Photon Calcium Imaging

The activity of cortical neurons was recorded by imaging fluorescence changes under a two-photon microscope (Bruker; Billerica, MA) excited with a Ti:Sapphire laser (Chameleon Ultra II; Coherent) tuned at 940 nm and scanned with resonant galvometers through a 20× (0.95 N.A.; Olympus) water immersion objective. To ensure stability of the imaging meniscus for long duration imaging sessions, a small volume (approx. 1ml) of Aquasonic ultrasound gel (Parker Laboratories Inc.) was centrifuged and dolloped onto a moistened, thinned skull in lieu of water. Scanning and image acquisition were controlled by Prairie

View software (≈30 frames per second for 256 × 256 pixels, 200-225 um beneath the pial surface). On imaging days (before and after treatment) mice were allowed 1 hour on the wheel before imaging began. Imaging consisted of a visual stimulation condition (15 minutes), followed by 20-40 minutes of awake rest in a dark room with the monitor off. Data are reported on 18 mice (11 female, 7 PV-cre, 11 SOM-cre).

Both 2P-Ca2+ and LFP recording sessions occurred between 11am and 3pm. Mice were monitored by the experimenter to ensure they were awake during data collection. Locomotion was detected as voltage deflections in the photodarlington readout. While previous work has suggested that locomotion enhances visual processing in V1 in mice, most of our mice did not exhibit enough locomotion to enable thorough examination of this effect in our paradigm (< 10% of frames/trials in LFP). Therefore, when detected, frames or trials during locomotion periods were excluded along with the previous and subsequent 60 frames (2-seconds). Large eye movements are uncommon in mice except during periods of locomotion, and, since we also near full field visual stimulation, the input for the recorded V1 retinotopic subfields was likely unaltered across trials and conditions.

Visual Stimulation

Visual stimuli were generated using the MATLAB (MathWorks) Psychophysics Toolbox and displayed on a liquid crystal display monitor (19-inch diameter, 60-Hz refresh rate) positioned 15 cm from the right eye, roughly at 45° to the long axis of the animal (Fig. 1a). Stimuli were static full-field square-wave gratings (100% contrast, 0.04 cycles per degree) oriented in 2 separate orientations for the oddball paradigm (45deg and 135deg) or in 8 orientations for the many-standards control (30, 45, 60, 90, 120, 135, 150, 180 deg). Stimuli were presented for 500 ms followed by an interstimulus interval of 1000-1500 ms of mean luminescence gray screen. In the oddball sessions, the “standard” stimulus was presented at a minimum of 3 sequential trials, followed by a linearly increasing probability of the “target” stimulus on each successive trial to yield an overall 12.5% probability of targets. These sessions lasted 10 minutes, and were repeated with the “standard” and “target” stimuli reversed. In the many-standards sessions, stimuli of 6 separate orientations each occurred at random with a 12.5% probability in a session of 10 minutes.

Current source density analysis

LFP data were manually prescreened for excessive artifact (e.g. signal greater than 8 standard deviations) and aberrant trials were removed and noisy channels were interpolated if present (never more than 2, and never 2 adjacent channels). Data were then digitally filtered from 0.1 to 300Hz (bandpass least squares FIR) and with a 60Hz notch filter. Average current source density (CSD) was computed from either the average LFP (for Fig 1d) or on single trials and averaging across trials (number equalized across conditions; between 32 and 68) by taking the discrete second derivative across the electrode sites and interpolated to produce a smooth CSD map (Buzsáki et al., 2012; Niell and Stryker, 2008). Putative laminar subregions (3 adjacent channels) were defined based on CSD demarcations previously published and histologically verified in mouse V1 for each mouse separately based on average CSD plots (see supplement). Importantly, the presence of MMN-like responses and their D.R.E.A.D.D modulation did not appear to differ dramatically as

function of layer, so statistical analyses and subsequent conclusions focus more generally on local (but not layer specific) processing in a V1 column. That is, we calculated a rectified CSD for each “layer” domain and averaged across domains within each mouse for statistical comparisons (Fig. 1,2). Average CSD waveforms were then averaged over stimulus orientations.

Image Analysis

Imaging datasets were scored similarly to previous reports (see supplement). ROIs were selected using a semi-manual PCA-assisted algorithm with halo subtraction (see supplement). The discrete first derivative on lowess-smoothed tracese was scored as delta-f (within cell/single cell comparisons). A 2-10 second baseline window was manually selected for each which contained no apparent calcium transients. The mean and standard deviation was calculated on the delta-f values in this window for each cell for the whole experiment which was used to i) compute a z-scored delta-f for visualizing and combining activity across cells and ii) determine activation thresholds (see supplement).

Single cell analyses

Condition averages of normalized delta-f values for redundant (4^{th} in sequence), deviant, and control stimuli were calculated separately for each stimulus type for each neuron. All analyses focused on the first 10-trials to equate across conditions, cells, and mice with varying numbers of available trials. Initial analyses focused on neurons showing, during control or deviant conditions, an average post-stimulus (0-1second) response of 1.67 stdevs above prestimulus baseline (equating to a 1-tailed p-value of .05; n=160, or 18.9% of all imaged cells; “Responsive” cells). Only responses to one stimulus orientation were considered for each cell (i.e. the orientation with greater magnitude). A minority of mice expressed GCaMP6f (5; 3 SOM-cre) while the rest expressed GCaMP6s (see supplement).

Pharmacogenetic suppression of interneurons

On the day of recording, mice viewed visual stimuli with intermittent “rest” periods as described above. Then hM4D-SOM mice and an equivalent number of control mice each received a subcutaneous injection of Clozapine N-Oxide (CNO; 12 mg/kg; within the range of previously reported doses (Roth, 2016; see supplement)), followed by a repeat of visual stimuli and “rest” periods during imaging or LFP recording 30 minutes later. In the presence of CNO, hM4D(Gi) activation functionally silences host cells primarily through the suppression of synaptic current amplitude and release (Roth, 2016).

Statistical procedures

All significance values for t-tests are two-tailed.

For establishing the presence of MMN-like potentials: the cross trial average LFP response from 40 to 240ms post-stim was averaged within mice and compared between redundant and deviant stimuli with a paried-samples t-test. SSA and deviance detection were confirmed with CSD and 2P-Ca2+.

CSD: Paired t-tests were computed on mouse-wise averages. For SSA we compared responses between control and redundant stimuli (using the 4th redundant in order to normalize for trial counts and for relative time during the run) in the early time-range (40-80ms). For deviance processing, we compared responses between deviant and control stimuli in the late time-range (120-240ms) (Chen et al., 2015a).

2P-Ca2+: Responses were quantified as described above (in **Single cell analyses).** Initial demonstration of SSA and deviance detection were established with paired t-tests on cell-wise averages of post stimulus activity (0-1 sec) from "responsive" cells. For SSA we compared responses between redundant and control stimuli; for deviance processing, we compared responses between deviant and control stimuli. Trial numbers were equated between stimulus conditions. All standard error bars in all figures reflect within-subjects/ within-cells standard error.

For determining the effect of SOM-suppression, a slightly different statistical approach was employed.

LFP/CSD: For LFP estimates of MMN (deviant minus redundant responses, 120-240 ms time range), CSD estimates of SSA (redundant minus control; 40-80ms), and CSD estimates of deviance detection (deviant minus control; 120-240ms), difference values for each mouse were subjected to a 2-by-2 mixed ANOVA with GROUP (CNO-control; SOM-hM4D) as the between subject variable and TREATMENT (pre/post) as the within subject variable were computed. One-way repeated measures ANOVAs within groups were used to describe interaction effects. As an exploratory step we next focused on stimulus evoked oscillatory power in the LFP of the SOM-hM4D group, and for SSA and deviance detection separately and for each frequency band, we carried a 2-by-2 repeated measures ANOVA on evoked power within mice with STIM (redundant or deviants; control) and TREATMENT (pre/post) as within subject variables. Follow-up paired t-tests for interactions were computed within treatment conditions.

2P-Ca2+: two complimentary statistical approaches tested for single cell effects of SOM suppression. First, focusing on "responsive cells" during the main SSA time window (0-500ms post-stim, control only; number of cells: CNO-controlpre/post=60/63; SOM-hM4Dpre/post=60/60), we computed the proportion of cells showing a redundant response of less than X stdevs below the control response average (for X=.25 to 2.5). Then, focusing on "responsive" cells during the main deviance detection time window (150-750ms post-stim, control or deviant; number of cells: CNO-controlpre/post=82/90; SOM-hM4Dpre/post=100/103), we computed the proportion of cells showing a deviant-stimulus response of greater than X stdevs above the control reponse average for X=.25 to 2.5 in 0.1 stdev steps. Thus each of the 4 conditions (pre/post; control/SOM) had one SSA curve and one deviance detection curve. We then computed a log-rank test on these curves for SSA and deviance detection separately, and for CNO-control and SOM-hM4D separately. Second, we focused on the cells with the top 10% magnitude average responses to the control stimulus (for SSA) or to the deviant stimulus (for deviance detection) in the pre-treatment run. Responses to the redundant stimulus and responses to the deviant stimulus were divided by the average response to the control stimulus for each of the 4 conditions. Then, separately for SSA and

DEV, a 2-by-2 mixed ANOVA on individual cells with GROUP (CNO-control; SOM-hM4D) as the between subject variable and TREATMENT (pre/post) as the within subject variable was computed. One-way repeated measures ANOVAs within groups were used to describe interaction effects. Pre-normalized values were also reported in figure S4, confirming the effects did not depend on changes in baseline response magnitudes.

Supplementary Material

Refer to Web version on PubMed Central for supplementary material.

Acknowledgements

We thank Azadeh Hamzei for technical support and Drs. Daniel Javitt, Darcy Peterka, and Reka Letso for comments. This work was supported by F32-MH106265, DP1EY024503, R01EY011787, DARPA SIMPLEX N66001-15-C-4032 and seedling W91NF-14-1-0269, ARO W911NF-12-1-0594 (MURI) and NARSAD.

References

Buzsáki G, Anastassiou CA, Koch C. The origin of extracellular fields and currents--EEG, ECoG, LFP and spikes. Nat. Rev. Neurosci. 2012; 13:407–420. [PubMed: 22595786]

Chen I-W, Helmchen F, Lütcke H. Specific Early and Late Oddball-Evoked Responses in Excitatory and Inhibitory Neurons of Mouse Auditory Cortex. J. Neurosci. 2015a; 35:12560–12573. [PubMed: 26354921]

Chen N, Sugihara H, Sur M. An acetylcholine-activated microcircuit drives temporal dynamics of cortical activity. Nat. Neurosci. 2015b; 18:892–902. [PubMed: 25915477]

Clementz BA, Sweeney JA, Hamm JP, Ivleva EI, Ethridge LE, Pearlson GD, Keshavan MS, Tamminga CA. Identification of Distinct Psychosis Biotypes Using Brain-based Biomarkers. Am. J. Psychiatry. 2016 In press.

Cottam JCH, Smith SL, Häusser M. Target-specific effects of somatostatin-expressing interneurons on neocortical visual processing. J. Neurosci. 2013; 33:19567–19578. [PubMed: 24336721]

Farley BJ, Quirk MC, Doherty JJ, Christian EP. Stimulus-specific adaptation in auditory cortex is an NMDA-independent process distinct from the sensory novelty encoded by the mismatch negativity. J. Neurosci. 2010; 30:16475–16484. [PubMed: 21147987]

Featherstone RE, Shin R, Kogan JH, Liang Y, Matsumoto M, Siegel SJ. Mice with subtle reduction of NMDA NR1 receptor subunit expression have a selective decrease in mismatch negativity: Implications for schizophrenia prodromal population. Neurobiol. Dis. 2015; 73:289–295. [PubMed: 25461194]

Garrido MI, Kilner JM, Stephan KE, Friston KJ. The mismatch negativity: a review of underlying mechanisms. Clin. Neurophysiol. 2009; 120:453–463. [PubMed: 19181570]

Gentet LJ, Kremer Y, Taniguchi H, Huang ZJ, Staiger JF, Petersen CCH. Unique functional properties of somatostatin-expressing GABAergic neurons in mouse barrel cortex. Nat. Neurosci. 2012; 15:607–612. [PubMed: 22366760]

Harms L, Michie PT, Näätänen R. Criteria for determining whether mismatch responses exist in animal models: Focus on rodents. Biol. Psychol. 2015

Hashimoto T, Bazmi HH, Mirnics K, Wu Q, Sampson AR, Lewis DA. Conserved regional patterns of GABA-related transcript expression in the neocortex of subjects with schizophrenia. Am. J. Psychiatry. 2008; 165:479–489. [PubMed: 18281411]

Javitt DC, Freedman R. Sensory processing dysfunction in the personal experience and neuronal machinery of schizophrenia. Am. J. Psychiatry. 2015; 172:17–31. [PubMed: 25553496]

Karnani MM, Agetsuma M, Yuste R. A blanket of inhibition: functional inferences from dense inhibitory connectivity. Curr. Opin. Neurobiol. 2014; 26:96–102. [PubMed: 24440415]

Light GA, Näätänen R. Mismatch negativity is a breakthrough biomarker for understanding and treating psychotic disorders. Proc. Natl. Acad. Sci. U. S. A. 2013; 110:15175–15176. [PubMed: 23995447]

Moran LV, Hong LE. High vs low frequency neural oscillations in schizophrenia. Schizophr. Bull. 2011; 37:659–663. [PubMed: 21653278]

Natan RG, Briguglio JJ, Mwilambwe-Tshilobo L, Jones S, Aizenberg M, Goldberg EM, Geffen MN. Complementary control of sensory adaptation by two types of cortical interneurons. Elife. 2015; 4

Niell CM, Stryker MP. Highly selective receptive fields in mouse visual cortex. J. Neurosci. 2008; 28:7520–7536. [PubMed: 18650330]

Roth BL. DREADDs for Neuroscientists. Neuron. 2016; 89:683–694. [PubMed: 26889809]

Womelsdorf T, Valiante TA, Sahin NT, Miller KJ, Tiesinga P. Dynamic circuit motifs underlying rhythmic gain control, gating and integration. Nat. Neurosci. 2014; 17:1031–1039. [PubMed: 25065440]

Zhu Y, Qiao W, Liu K, Zhong H, Yao H. Control of response reliability by parvalbumin-expressing interneurons in visual cortex. Nat. Commun. 2015; 6:6802. [PubMed: 25869033]

Highlights

-Visual mismatch negativity (MMN, reduced in schizophrenia) is reproduced in awake mice

-Two MMN components (adaptation and deviance detection) are differentiated in neurons

-Silencing somatostatin interneurons (SOMs) specifically impairs deviance detection

-Silencing SOMs also alters theta/alpha MMN frequency activity, like in patients

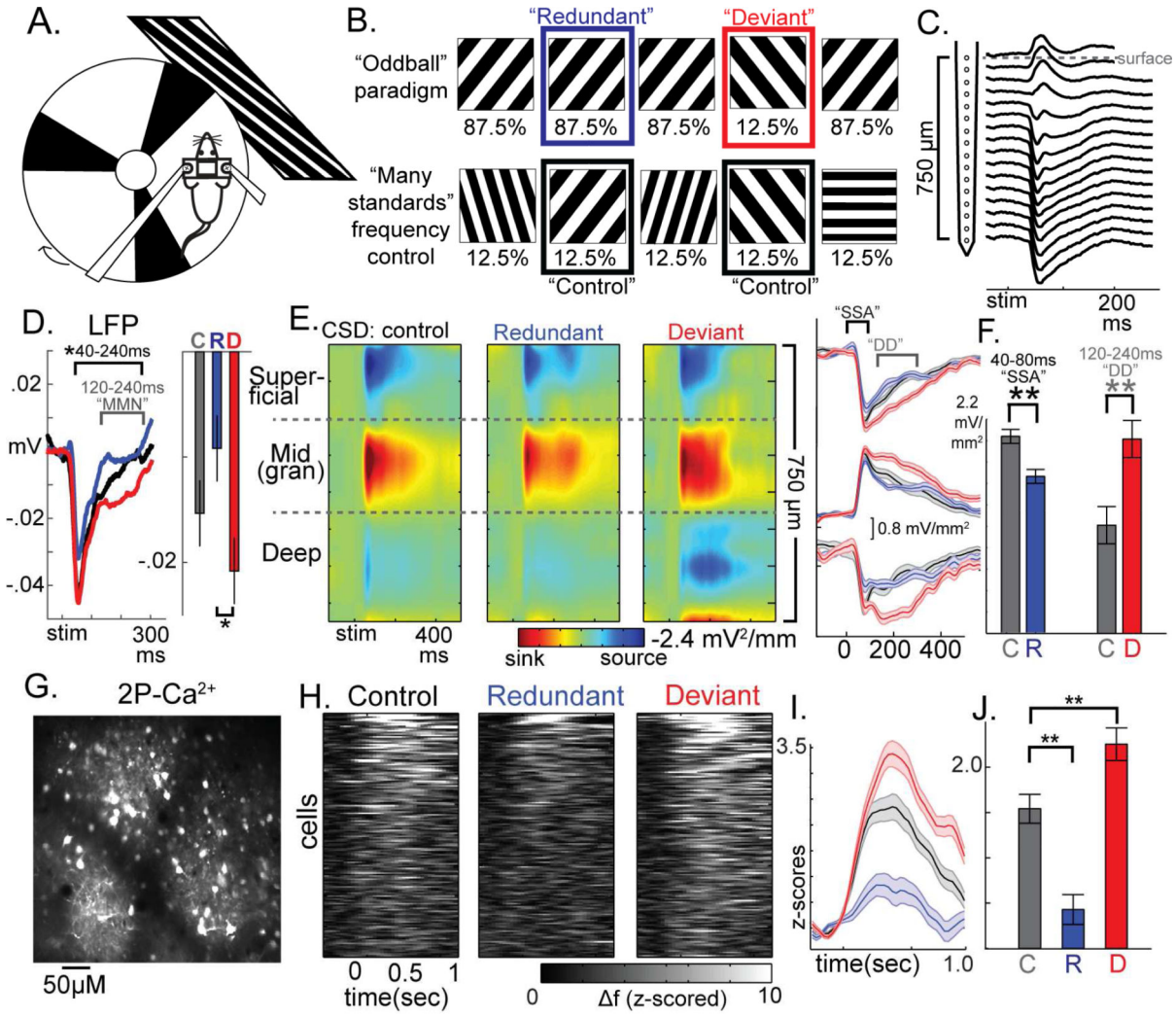

Figure 1. Circuit-level components of Mismatch Negativity are present in visual cortices of awake mice

(a) Head-fixed mice viewed square-wave gratings while running on a treadmill during (b) oddball and many-standards control of stimulus frequency. (c) 16-channel multielectrode recordings in left visual cortex reveal (d) a significant "deviant" vs "redundant" effect in the peak LFP channel with a similar timecourse to human MMN. (e) Current source density profiles with an initial large current sink occurring in putative granular layer evinced stimulus-specific adaptation (SSA) and deviance detection (DD) across all depths (averaged over orientations). (e,f) significant SSA occurred early (40-80ms) while DD occurred later (120-240ms; plots in c-f are cross animal averages. Bars reflect area under the curve (A.U.C.) for these time ranges averaged across all depths). (g, h) two-photon calcium imaging of GCaMP6 expressing cells demonstrate (h,i,j) SSA and DD in the 19% neurons significantly activated by stimuli (only response to preferred stimulus plotted/analyzed for each cell; i, averaged across 159 neurons, 0-1 sec A.U.C.). **p<.01. All error bars S.E.M.

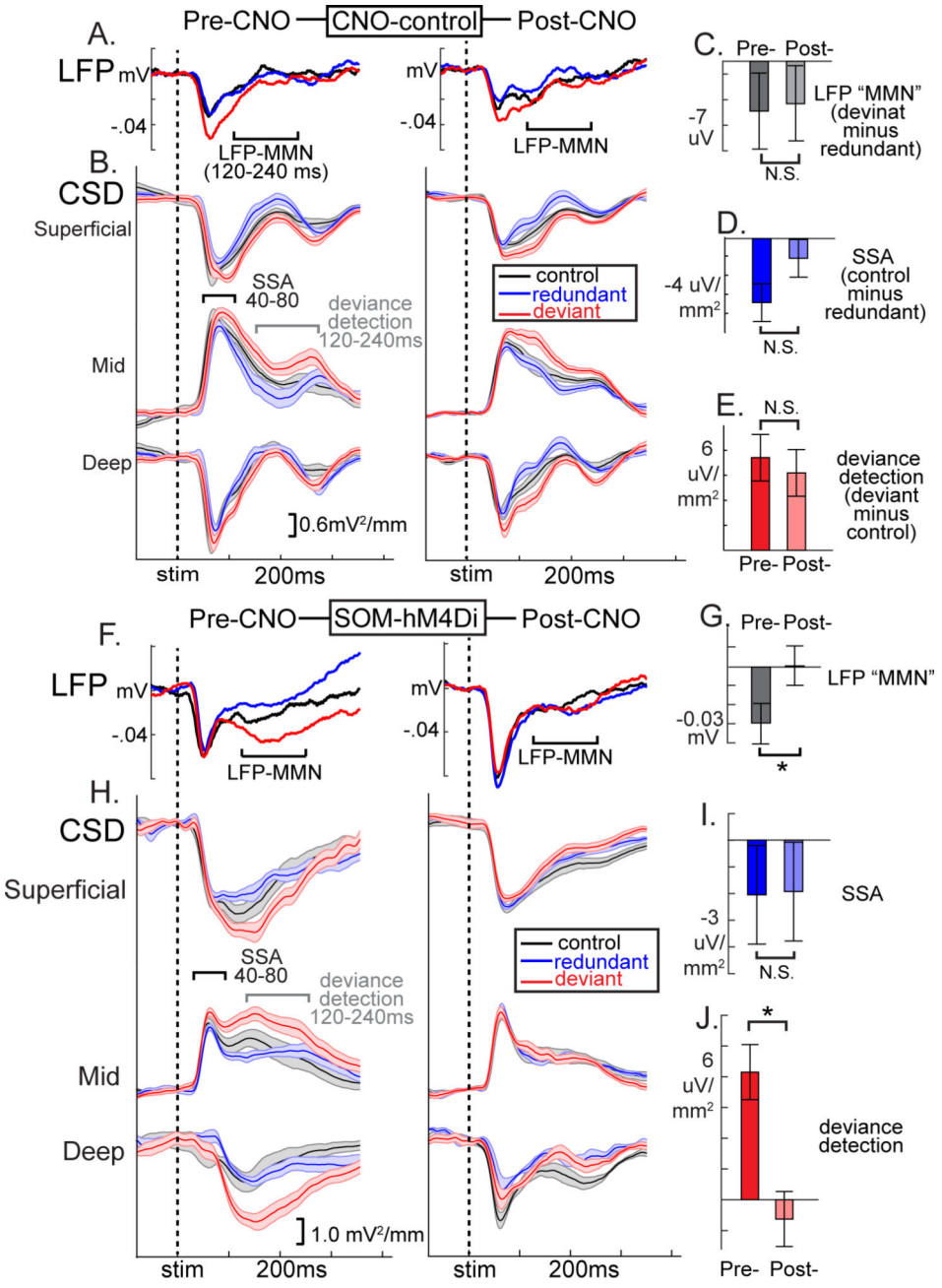

Figure 2. Suppression of somatostatin interneurons diminishes deviance processing in LFP and CSD measurements

Grand-averaged (a) LFP and (b) CSD waveforms (across mice and 40-60 trials) in the CNO-control condition before and after CNO injection confirm the stability of (c) mismatch negativity-like potentials (deviant minus redundant, 120-240ms post-stim), (d) SSA (control-minus deviant; 40-80ms), and (e) deviance detection (deviant minus control; 120-240ms; n=4 mice; all p>.30). hM4Di mediated suppression of SOMs (f,g) disrupted LFP-MMN difference potentials. (h) In the CSD, (i) SSA was not affected, but (j) deviance detection was abolished (n=5 mice; $F(4)=7.51$, *p<.05; bars reflect area under the curve, averaged across all depths)). All error bars S.E.M.

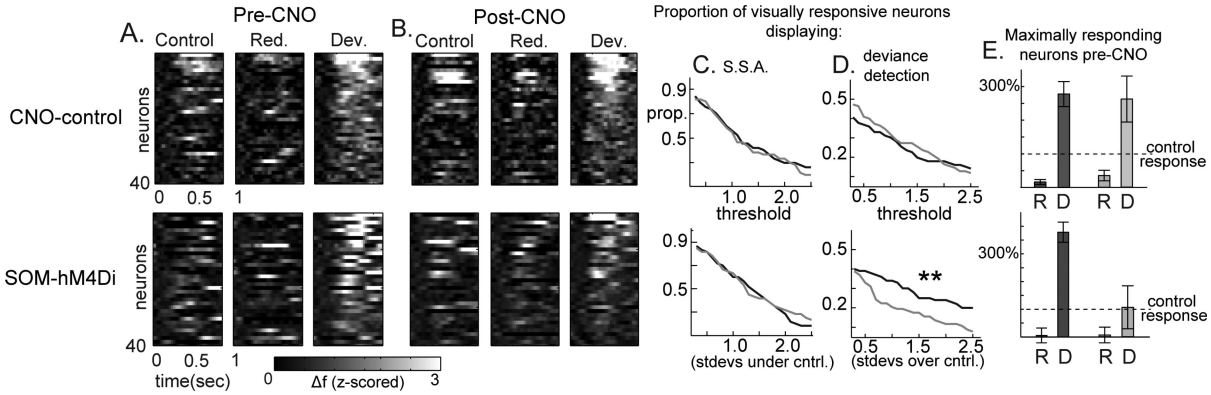

Figure 3. Suppression of somatostatin interneurons reduces MMN in two-photon calcium imaging measurements

Compared to the CNO-control (above), (a,b) SOM-suppression reduced early and late deviance detection responses in individual neurons. (c,d) The proportion off all visually responsive neurons showing deviance detection, but not SSA, was reduced across thresholds. (e) This pattern held also when focusing on the top 10% of pre-treatment neurons showing the largest average responses (normalized to pre-CNO control stimulus response).

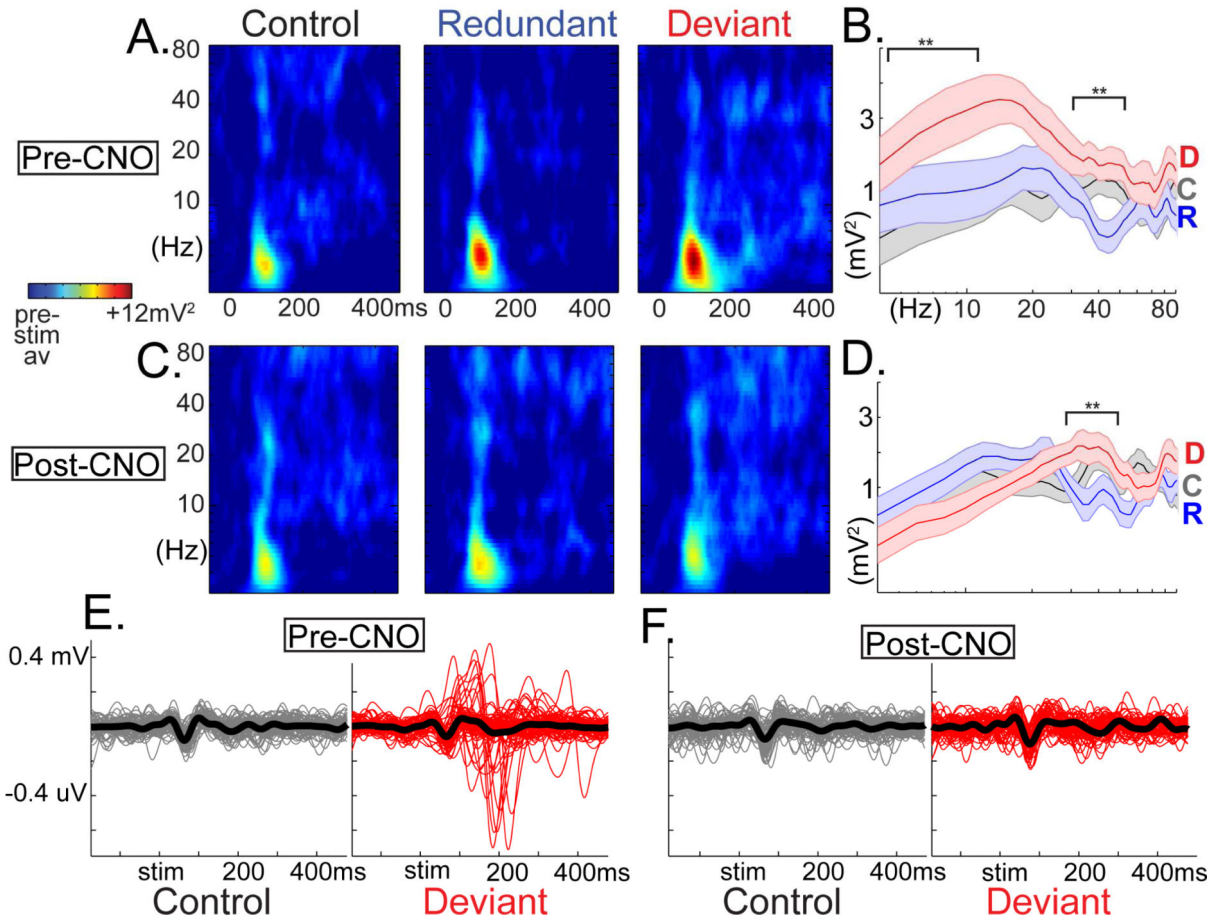

Figure 4. Somatostatin interneurons influence salience processing in low but not high frequency bands

LFP data converted to time/freq domain. (a) Log-scaled time-frequency spectra averaged across trials (<50) and 5 mice for each condition, and (b) averaged across post-stim time-points (30-450ms) show that deviant stimuli augment low-frequency induced power (relative to control) while low-gamma power is suppressed to redundant stimuli. (c-d) The former effect is absent after SOM-suppression, while the latter is not. Note that the magnitudes of control and redundant oscillatory power are nominally unchanged by SOM-suppression (scales are constant across all plots). (e-f) Low-pass filtered (4-14Hz) single trial traces show that deviant elicited low-freq enhancement lasts 1-2 cycles, is not phase locked, and is suppressed after SOM suppression (from 1 representative mouse). **p<.01. All error bars S.E.M.